Applied Catalysis B: Environmental 305 (2022) 121044

Contents lists available at ScienceDirect

Applied Catalysis B: Environmental

journal homepage: www.elsevier.com/locate/apcatb

Increasing the utilization of SiBeta support to anchor dual active sites of transition metal and heteropolyacids for efficient oxidative desulfurization of fuel

Lei Chen, Jin-Tao Ren, Zhong-Yong Yuan *

Key Laboratory of Advanced Energy Materials Chemistry (Ministry of Education), School of Materials Science and Engineering, Nankai University, Tianjin 300350, China

ARTICLE INFO

Keywords:
Oxidative desulfurization
Supported metal-based catalysts
Heteropolyacids
Synergistic effect

ABSTRACT

Aiming at improving the activity of supported catalysts toward oxidative desulfurization (ODS) reaction, an increasing support utilization rate strategy is developed by introducing additional phosphotungstic acid (HPW) on V anchored zeolite SiBeta. Both the Keggin HPW on the surface of SiBeta and the tetrahedral V species into the framework of SiBeta possess high intrinsic catalytic activity for the oxidation of sulfides. Grafting V species into the framework of SiBeta can create Lewis acid sites and HPW serves as a typical source of Brønsted acidity, while the synergistic effect between Lewis and Brønsted acids contributes to the formation of numerous peroxometallate complexes with strong oxidizing capacity. The obtained catalyst exhibits outstanding catalytic performance toward ODS reaction and can adsorb ODS products, thus removing them from oil phase. In addition, series of efficient catalysts were prepared by adjusting the types of heteropolyacids and transition metal (V, Ti, Nb and Zr) to control their acidity. It is indicated that the ODS activity is favored by the enhancing the strength and density of Lewis acid sites and the density of Brønsted acid sites. Such concepts of engineering both increasing support utilization and synergistic effect of dual-active sites herald a new paradigm for the construction of supported catalysts.

1. Introduction

The crude oil contains a high content of refractory sulfur compounds (about 5 wt%), and the SO_x caused by the combustion of sulfur compounds have adverse industrial and environmental effects including the formation of acid rain and air pollution [1]. Increasingly serious and alarming environmental issues force to adopt more stringent emission standards on the sulfur content in transport oil [2]. Oxidative desulfurization (ODS) has been frequently regarded as the most promising desulfurization technique due to the mild and simple operation conditions as well as the high efficiency on the removal of stubborn aromatic sulfur compound including dibenzothiophene (DBT), benzothiophene (BT) and 4,6-dimethyldibenzothiophene (4,6-DMDBT) [3].

During the ODS process, the sulfide moiety in DBT can be oxidized by a suitable oxidant in the presence of catalysts, producing easily separable sulfone with less toxicity [4]. The catalysts in the ODS reaction can activate the oxidant to boost the generation of active oxygen species ($^{\cdot}OH$, O_2^- and metal peroxygen species), thereby the speed of the ODS process can be increased [5]. Hitherto, numerous heterogeneous catalysts including transition metal oxides (TMOs) [6], heteropolyacids (HPAs) [7], zeolites [8], metal organic frameworks (MOFs) and metal-free catalysts have shown impressive performances in ODS [9]. Among them, dispersing TMOs and HPAs active centers on the porous supports with high specific surface area to obtain highly efficient ODS catalysts has been considered as a research hotspot in recent years [10, 11].

The large surface area and well-ordered channel system endow zeolite with great potential to serve as an excellent candidate of catalyst support in ODS reactions [12]. Gonzalez et al. synthesized a series of WO_3/SBA-15 catalysts using SBA-15 as support, finding that the concentration of oxygen defects and Lewis acid sites in the crystalline structure of WO_3 increased significantly as the loading amount of WO_3 increases [13]. The optimal catalyst 25 wt%WO_3/SBA-15 with the largest amount of oxygen defects and Lewis acid can remove more than 99% of 4,6-DMDBT within 15 min. However, such high metal loading amount will inevitably increase the cost and the leaching of active metal

* Corresponding author.
E-mail address: zyyuan@nankai.edu.cn (Z.-Y. Yuan).

https://doi.org/10.1016/j.apcatb.2021.121044
Received 10 August 2021; Received in revised form 7 December 2021; Accepted 23 December 2021
Available online 27 December 2021

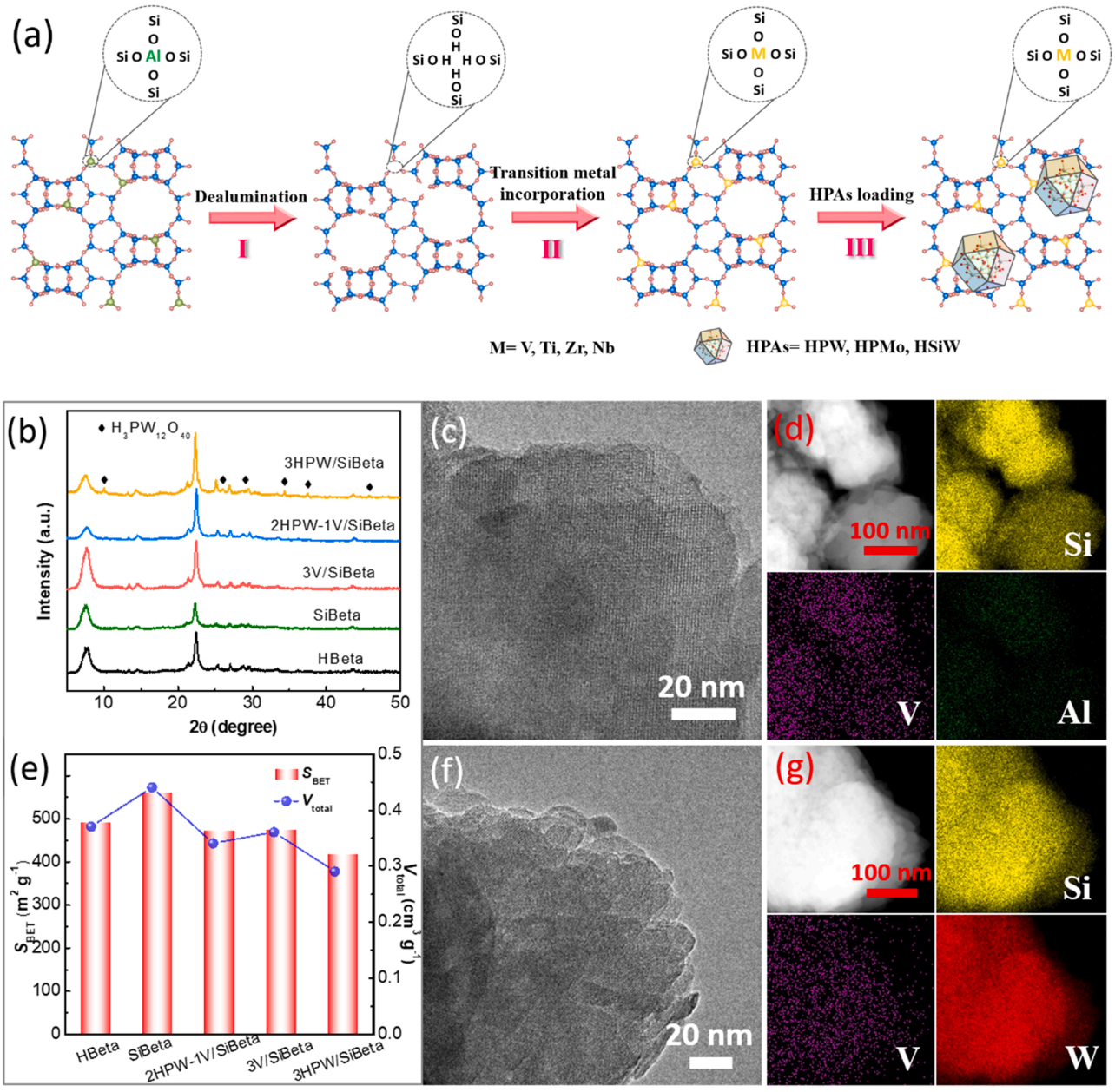

Fig. 1. (a) Schematic illustration of the preparing process of *y*HPAs-*x*M/SiBeta. (b)The XRD patterns of the obtained samples. (c) TEM and (d) EDS elemental mapping images of 1 V/SiBeta. (e) BET surface areas and pore volume of the obtained samples. (f) TEM and (g) EDS elemental mapping images of 2HPW-1 V/SiBeta.

from the support leads to the secondary heavy metal pollution of fuel oil. SiBeta, formed by zeolite Beta after dealumination by acid-leaching, has a myriad of vacant T-sites to accommodate metal species (ions or oxides etc.) through the interaction between metal and silanol groups [14,15]. The metal active components are generally downsized into nanoparticles and firmly distributed on the SiBeta support, which can enhance the exposure and stability of metal active sites during the reaction [16]. As reported, group ⅣB (Ti and Zr) and group ⅤB (Nb and Ta) metals supported on SiBeta have great potential to activate oxidants with relatively low metal content for the efficient oxidation of organosulfur species in fuel oil [17,18]. Optimizing the utilization of active metal has been considered as a pivotal goal to construct the metal-based supported catalysts for a prolonged period of time. When the metal loading amount reaches a certain value, continuing to add the same metal species to the support will cause aggregation, decreasing the utilization of metal active sites. Introducing another active component, whose location on the support is different from the first active one, can not only meet the requirement of uniform dispersion of two active components but also create a synergistic effect to improve the catalytic performance [19]. However, this has not been investigated to rationalize the utilization rate of the support to further improve the catalytic activity when the metal utilization is close to (or has reached) the optimum.

Herein, we report an increasing support utilization rate strategy to load phosphotungstic acid (HPW) on V anchored SiBeta for the efficient ODS reaction. Most of V species and bulky Keggin HPW exist in the framework and on the surface of SiBeta, respectively, and both of them are uniformly dispersed. HPW possesses Brønsted acidity and V species coordinated with silanol groups in the vacancies left by Al atoms can provide Lewis acid sites, which permit the coexistence of Lewis and Brønsted acid sites to facilitate the generation of peroxometallate complexes with high oxidizing capability. Benefiting from the structural merits, the high intrinsic activity of HPW and tetrahedral V species, and the synergy between Lewis and Brønsted acids, the obtained catalyst

2HPW-1 V/SiBeta exhibits remarkable catalytic activities and stability for ODS reaction, far ahead of HPW/SiBeta and V/SiBeta. Simultaneously, over 80% of oxidation products ($DBTO_2$) can be adsorbed and removed by interaction with silanol groups in the catalysts, which reduces the need for the following extraction step to obtain ultralow sulfur fuel. To get insight into the effect of acidity on catalytic efficiency, series of efficient catalysts with different acidity were prepared by adjusting the types of HPAs and transition metal (V, Ti, Nb and Zr). The characterization and experimental results suggest that enhancing the strength and density of Lewis acid sites and the density of Brønsted acid sites are essential for the improvement of ODS activity.

2. Experimental section

2.1. Catalyst preparation

Dealumination of HBeta zeolite (SiO_2/Al_2O_3 ratio of 25, Tianjin Shenneng) was carried out in a 13 M HNO_3 solution (20 mL $g_{zeolite}^{-1}$) at 100 °C for 12 h to remove Al completely. Subsequently, the suspended solid was centrifuged and washed with deionized water copiously to remove residual HNO_3 species, followed by drying in the vacuum oven (temperature of 200 °C, internal pressure of −0.1 MPa) overnight to remove water. After that, the calculated SiBeta and ammonium vanadate (NH_4VO_3, Adamas Reagent) were added into an appropriate amount of deionized water with continuous stirring for 12 h. The solid mixture was dried at 80 °C and then calcined under flowing air at 550 °C for 2 h. The as-obtained samples were marked as *x*V/SiBeta, where *x* represents the weight percent of V content.

Keggin structure HPAs including phosphotungstic acid (HPW, Tianjin Guangfu), silicotungstic acid (HSiW, Tianjin Guangfu) and phosphomolybdic acid (HPMo, Tianjin Guangfu) with the calculated amount was dissolved in 10 mL deionized water, then 0.5 g V/SiBeta or SiBeta was dispersed into the solution under vigorous stirring to evaporate the solvent. The collected solid product was dried at 80 °C and denoted as *y*HPAs-V/SiBeta or *y*HPAs/SiBeta, where *y* refers to the weight percent of metal content in SiBeta (W for HPW and HSiW, and Mo for HPMo).

For comparison, Ti/SiBeta, Nb/SiBeta and Zr/SiBeta were synthesized by the identical method as V/SiBeta, where tetrabutyl titanate ($C_{16}H_{36}O_4Ti$, Tianjin Guangfu), zirconium nitrate ($Zr(NO_3)_4{\cdot}5H_2O$, Tianjin Guangfu) and niobium oxalate ($C_{10}H_5NbO_{20}$, Shanghai D&B) were used as metal sources, and the deionized water solvent was replaced by absolute ethanol for $C_{16}H_{36}O_4Ti$. Moreover, series of *y*HPAs-*x*M/SiBeta catalysts were fabricated by the same procedure as above (HPAs= HPW, HSiW and HPMo, M = Ti, Zr, V and Nb).

2.2. Catalyst characterization

X-ray diffraction (XRD) patterns were recorded on a Rigaku SmartLab diffractometer with Cu *K*α radiation. Transmission electron microscopy (TEM) and electron energy dispersive spectroscopy (EDS) were carried out on a Jeol JEM-2800 microscope at 200 kV. Thermogravimetry analysis (TGA) was performed on a TA Q600 SDT instrument with a heating rate of 10 °C min^{-1} and air flow rate of 100 mL min^{-1}. N_2 adsorption-desorption analysis was carried out on a Quantachrome Nova 2000e sorption analyzer at 77 K. The specific surface area (S_{BET}) was calculated by the Brunauer-Emmett-Teller (BET) method, the pore size distribution curves were obtained from the adsorption branch of the isotherms according to the nonlocal density functional theory (NLDFT) method, and the total pore volume (V_{total}) was determined at the relative pressure of $P/P_0 = 0.99$. UV–vis spectra were measured on a Shimadzu 2450 spectrometer, using $BaSO_4$ as the reference. Fourier transform infrared (FT-IR) spectra were measured on a Bruker VECTOR 22 spectrometer with KBr pellet technique. X-ray Photoelectron Spectroscopy (XPS) was carried out on a Kratos Axis Ultra DLD spectrometer equipped with a monochromatic Al *K*α X-ray source (1486.6 eV).

2.3. Catalytic testing

0.1 g of DBT (Aladdin) was dissolved in 99.9 g of decalin (Meryer) to obtain 1000 ppm model oils. The typical ODS process was carried out in a glass reactor including 10 mL model oil, 0.02 g catalysts and a certain amount of tert-butyl hydroperoxide (TBHP, 70%, Adamas Reagent) with TBHP/DBT (O/S) molar ratio of 3. The mixture was stirred vigorously and heated to 60 °C. During the ODS reaction, the liquid phase oil at intervals 5 or 10 min was sampled and analyzed on a gas chromatograph equipped with an FID detector. The DBT conversion was calculated by the following equation:

$$\alpha = \frac{C_0 - C_t}{C_0} \times 100\% \quad (1)$$

where α is the DBT conversion (%); C_0 and C_t are the DBT content in the beginning and after *t* min desulfurization reaction, respectively.

3. Results and discussion

3.1. Material synthesis and characterization

The strategy of increasing support utilization rate is proposed to fabricate *y*HPAs-*x*M/SiBeta catalysts. As shown in Fig. 1a, the synthesis of *y*HPAs-*x*M/SiBeta contains three successive steps: (I) the dealumination of HBeta zeolite to prepare SiBeta with abundant vacancies, (II) the incorporation of transition metal with appropriate loading amount into the SiBeta framework for the formation of M/SiBeta, (III) the further introduction of HPAs on the M/SiBeta to obtain the *y*HPAs-*x*M/SiBeta. Due to the silanol nests uniformly distributed on the SiBeta can coordinate with metal precursors, the metal atoms can be stabilized into the framework of SiBeta uniformly after calcination [15]. When the metal loading amount in M/SiBeta reaches a certain value, the further addition of the same metal species will cause aggregation of metal components to decrease the utilization of metal active sites. Thereby, Keggin HPAs, another ODS active components, were further introduced into M/SiBeta to enhance the effective utilization of SiBeta support to improve the catalytic performance.

To investigate the crystal structure changes of Beta zeolites during the subsequent catalyst synthesis procedures, XRD analysis was initially performed. As shown in Fig. 1b, the typical BEA topology structure can be observed for all samples, suggesting that the characteristic frameworks may be intact after dealumination and the introduction of V and HPW. The differences in the diffraction peaks (302) of HBeta, SiBeta and 3 V/SiBeta detected at $2\theta = 22.45°$, 22.30° and 22.51°, respectively, can be attributed to the contraction/expansion of the framework resulting from the dealumination and the successful incorporation of V species into the framework of Beta [20]. Owing to most of V species are uniformly confined in the framework of SiBeta homogenously, there is no V-based diffraction peaks on the XRD pattern of 3 V/SiBeta [21]. On the contrary, HPW molecules mainly locate on the exterior surface of the Beta zeolite due to the bulk structure of HPW much larger than the pore window size of Beta, leading to the obvious appearance of diffraction peaks of the $H_3PW_{12}O_{40}$ crystallites in the 3HPW/SiBeta [19]. However, no diffraction peaks relate to the keggin-structure of HPW on the XRD patterns of 2HPW-1 V/SiBeta, which can be ascribed to the low loading amount of HPW.

The textural properties of the obtained samples can be reflected by N_2 adsorption-desorption isotherms. As shown in Fig. S2, all the samples exhibit the similar N_2 adsorption behavior to that of HBeta. The high N_2 uptake below low relative pressure ($P/P_0 < 0.1$) and the obvious adsorption at high relative pressure ($P/P_0 > 0.8$) relate to the typical micropores and the mesopores between interparticles, respectively [20]. Compared with the parent HBeta, the specific surface area and total pore volume increase slightly after dealumination (SiBeta) and decrease a bit after the incorporation of V (3 V/SiBeta), as shown in Fig. 1e. This

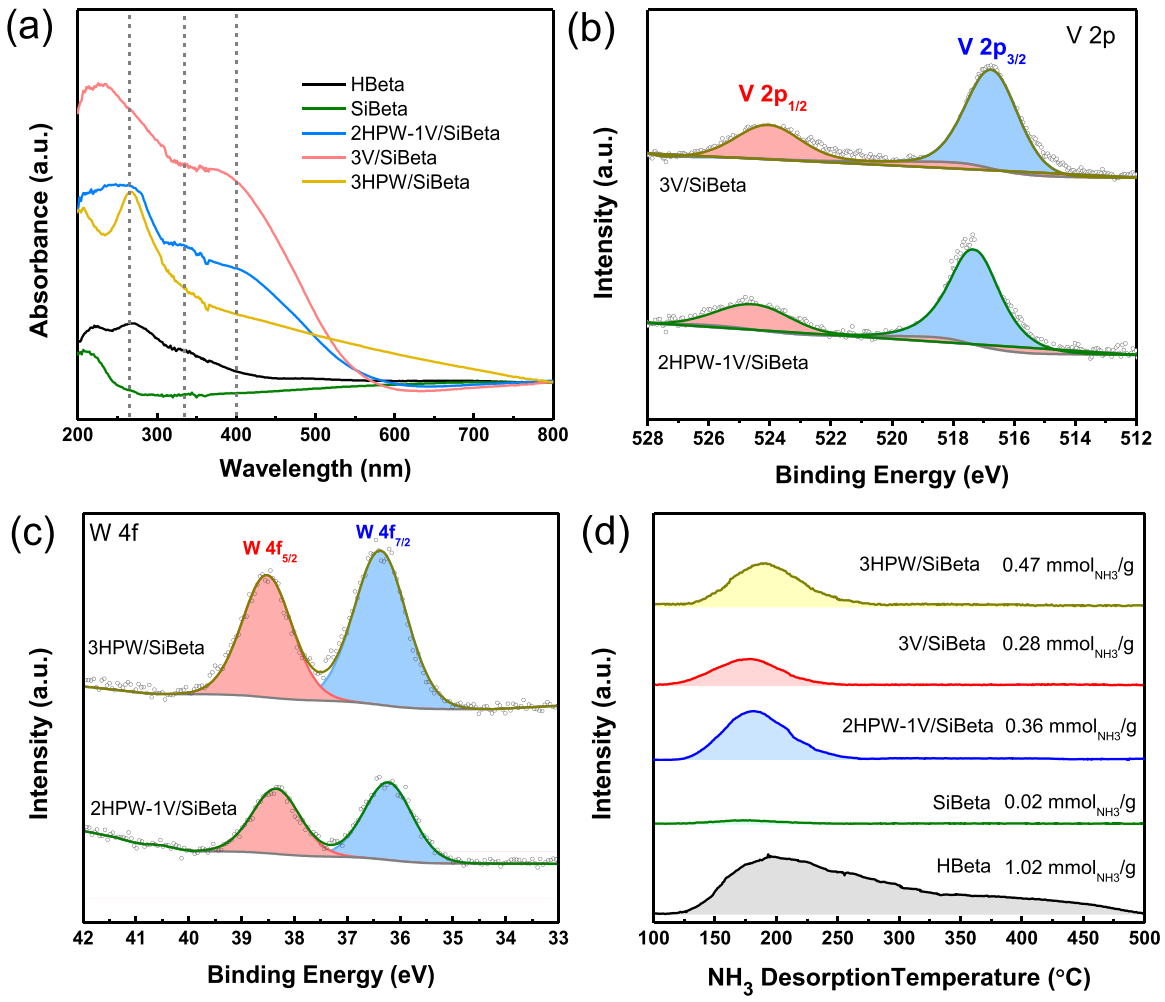

Fig. 2. (a) UV–vis spectra of HBeta, SiBeta, 3 V/SiBeta, 3HPW/SiBeta and 2HPW-1 V/SiBeta. (b) V 2p XPS spectra of 3 V/SiBeta and 2HPW-1 V/SiBeta. (c) W 4 f XPS spectra of 3HPW/SiBeta and 2HPW-1 V/SiBeta. (d) NH_3-TPD curves of HBeta, SiBeta, 3 V/SiBeta, 3HPW/SiBeta and 2HPW-1 V/SiBeta, with their corresponding acid density shown inside.

reveals that the abundant V species not only graft into the framework of SiBeta but also exist in the form of extra-framework VO_x oligomers to partially block the channels [22]. By comparing the textural properties of 3 V/SiBeta and 3HPW/SiBeta, it can be found that HPW possesses a stronger ability to block the channels of the support than V species due to its bulky structure. Thus, the surface area and pore volume of 2HPW-1 V/SiBeta with low amount of HPW are markedly superior to those of 3HPW/SiBeta.

The distribution of V and HPW on the surface of SiBeta was identified by TEM and EDS elemental mapping images. As shown in Fig. 1c, no obvious metal particles can be detected in 1 V/SiBeta under high-magnification TEM image, and the corresponding EDS mapping images indicate that V is highly dispersed throughout the whole SiBeta support. And the disappearance of Al species implies that most of Al species have been removed after acid treatment. After the further introduction of HPW, there are still no large metal particles observed in the TEM image of 2HPW-1 V/SiBeta (Fig. 1f) due to the low loading amount and uniform dispersion of metal active components. The EDS mapping images (Fig. 1g) further confirm that both the V and W are fairly homogenously dispersed on the zeolite surface, which is consistent with the XRD results.

The chemical coordination environment of V and HPW presented in the SiBeta support was characterized by DR UV–vis spectroscopy, and the results are shown in Fig. 2a. For 3 V/SiBeta, two main bands located at 265 and 340 nm can be assigned to oxygen-to-pseudo-tetrahedral V (V) charge transfer transitions, including bridging (V-O-Si) and terminal (V═O) oxygens, respectively [23]. This can corroborate the presence of tetrahedral V species into the framework of SiBeta [24], and such successful substitution of Al(III) in tetrahedral position with V(V) may be caused by the nearly identical ionic radius between them. The broad absorption near 400 nm is pertinent to the charge transfer transition from octahedral oxygen ligands to a central V(V) atom, which is the typical feature of extra-framework VO_x species [22]. The UV–vis spectrum of 3HPW/SiBeta exhibits two intense peaks at 202 and 260 nm, which are attributable to the Keggin-type HPW [25]. Compared with 3 V/SiBeta, the broader peak at 265 nm and the significantly decreased peak at 400 nm in the spectrum of 2HPW-1 V/SiBeta can be ascribed to the introduction of Keggin-type HPW and lower content of extra-framework VO_x species.

The surface chemical state and composition of 2HPW-1 V/SiBeta were explored by XPS analysis. As shown in Fig. 2b, the peaks corresponding to V $2p_{1/2}$ and V $2p_{3/2}$ of 3 V/SiBeta shift to the low binding energy direction as compared to that of bulk V_2O_5, which may be related to the successful graft of tetrahedral V into SiBeta framework, promoting the information of V-O-Si bond [21]. The similarity between V 2p spectra of 2HPW-1 V/SiBeta and 3 V/SiBeta suggests the introduction of HPW did not change the chemical state of V species. Notably, the binding energy of W 4f peaks in 3HPW/SiBeta has a positive shift compared with that of pure HPW (Fig. S3a), indicating the electron transfer from HPW to SiBeta. This phenomena can be ascribed to the

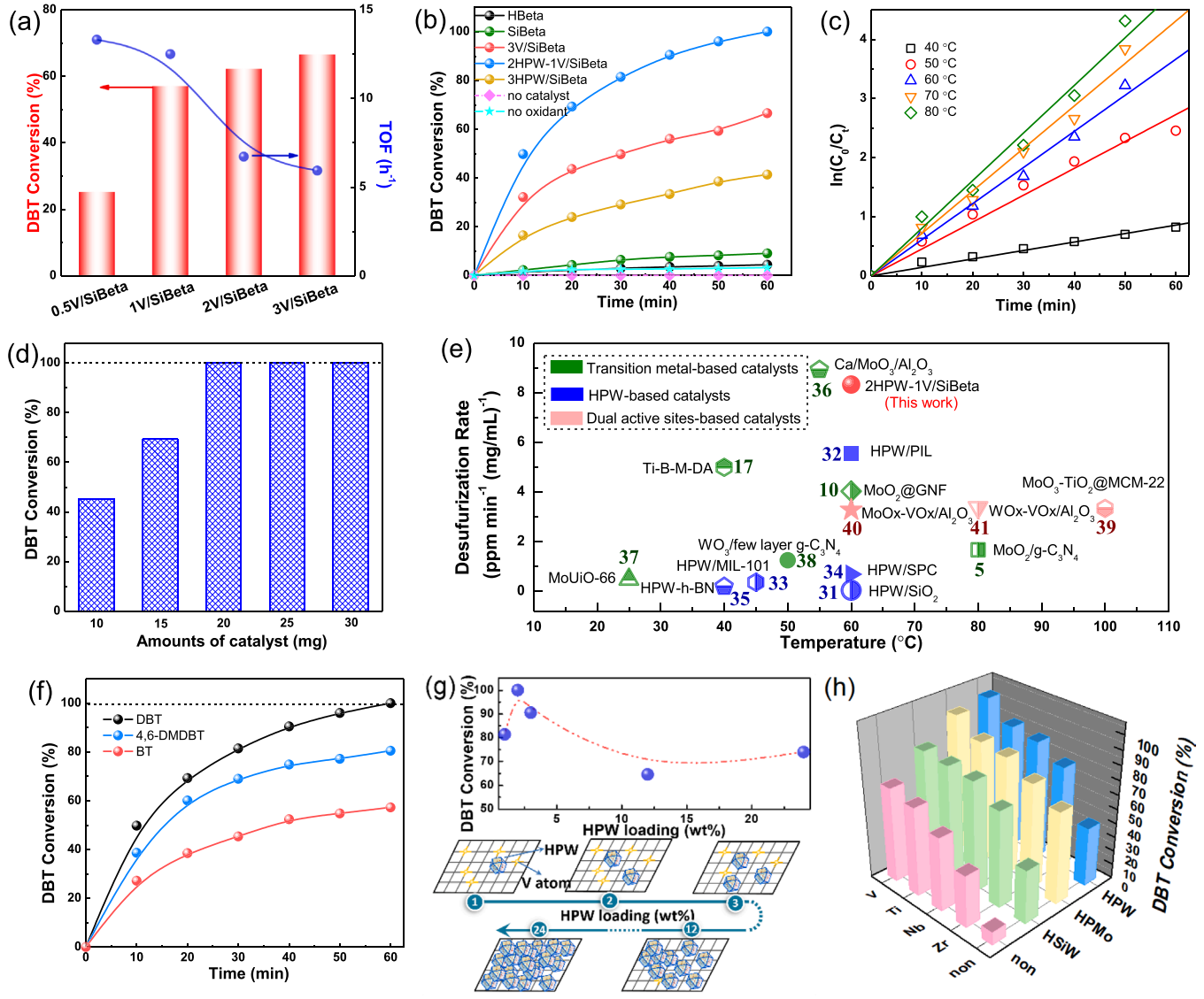

Fig. 3. (a) Catalytic performance of V/Beta with different V loading amounts for oxidation of DBT. (b) ODS activities of the obtained catalysts. (c) Pseudo-first-order rate constants for oxidation of DBT over 2HPW-1 V/SiBeta at different reaction temperatures. (d) Effect of 2HPW-1 V/SiBeta catalyst dosage on the oxidation of DBT. (e) Comparison of ODS activities of the supported catalysts in this work and in the literature. The desulfurization rate is calculated by that the concentration of DBT can be removed by per mg/mL of catalysts per minute. Effects of (f) different sulfides, (g) HPW loading amount and (h) different active components on the sulfur removal. (Experimental conditions: $T = 60$ °C, m(catalyst) = 20 mg, O/S = 3, $r = 800$ rpm, $t = 60$ min).

electron-rich characteristic of the Keggin HPW, which allows the terminal asymmetric oxygen to act as electron donors to transfer electrons to the nearby Si–OH on the surface of SiBeta [26]. In Fig. 2c, W 4f region of the 2HPW-1 V/SiBeta shows doublet peaks at 36.2 and 38.3 eV for W $4f_{7/2}$ and W $4f_{5/2}$ of HPW, which are accordant with that of 3HPW/Si-Beta, revealing that heteropolyanions are mainly combined with silica matrix (not vanadium) to form weak interaction effect between HPW and SiBeta support [27]. To further investigate the location of V sites and HPW in 2HPW-1 V/SiBeta, XPS depth profile was carried out. As shown in Fig. S3b, the intensity of W 4f peaks of 2HPW-1 V/SiBeta drops drastically after depth profile, indicating that most of HPW molecules are dispersed on the surface of SiBeta support. However, the intensity of V 2p peaks (Fig. S3c) is almost identical with the previous one, which can be ascribed to the same content of V on the surface and inside of the catalyst, further certifying that HPW on the surface of support did not cause the coverage of V sites. For 2HPW-1 V/SiBeta, V sites are bound to the silanol groups into the framework of SiBeta and HPW species are anchored to silica matrix on the surface of SiBeta, especially, V sites and HPW are separated from each other.

The surface acidity of the obtained samples can be quantified by NH_3-TPD analysis and shown in Fig. 2d. Two main peaks at 180 and 380 °C corresponded to the weak and medium acid sites in HBeta, respectively, are diminished significantly in SiBeta, which suggests that most of lattice Al atoms have been removed from the Beta framework after dealumination [14]. For 3 V/SiBeta, the introduction of V species into the SiBeta support can enhance the total acidity from 0.09 to 0.3 mmol NH_3/g. 3HPW/SiBeta exhibits a NH_3 desorption peak between 150 and 350 °C with a total acidity of 0.55 mmol NH_3/g, indicating that HPW has greater potential than V sites in improving the acidity of the whole catalyst [25,28]. And the total acidity of 2HPW-1 V/SiBeta is 0.34 mmol NH_3/g when the V active sites and HPW were simultaneously introduced into one catalyst.

3.2. Catalytic performance toward oxidative desulfurization

V/SiBeta with different loading amounts have been synthesized and

used in the catalytic oxidation of DBT (Fig. 3a). 1 V/SiBeta displays a significantly improved ODS activity than that of 0.5 V/SiBeta. Further increasing the V loading amount, the ODS activity of V/SiBeta increases gradually. 3 V/SiBeta can achieve the complete desulfurization in 120 min (Fig. S4) but the corresponding TOF values (calculated based on the DBT conversion at 5 min) decreased obviously, indicating the inferior utilization of V active sites. H_2-TPR and N_2 adsorption-desorption analysis were carried out to reveal the underlying causes of the above results. As shown in Fig. S5, H_2-TPR profiles of all *x*V/SiBeta consist of two reduction peaks in the range of 400–500 and 500–600 °C, which can be ascribed to extra-framework V species and tetrahedral V species into the framework of SiBeta, respectively [29]. When the loading amount of V exceeds 1%, further increasing the V concentration would greatly enhance the content of extra-framework V species. According to the previous reports, extra-framework V species possess the weaker oxidizing ability than that of tetrahedral framework V species [22,23]. Additionally, the excessive extra-framework V species caused by the high V loading amount can interact with each other to form oligomeric VO_x species, which would block the channels and lead to the decrease of specific surface area (Fig. S6). 1 V/SiBeta can realize the relatively efficient desulfurization rate with higher utilization of V active sites as compared with that of 0.5 V/SiBeta, 2 V/SiBeta and 3 V/SiBeta. Nevertheless, the ODS performance of 1 V/SiBeta still needs to be further improved.

In fact, there is still ample space to accommodate other active components on the surface of 1 V/SiBeta due to the low loading amount of V. Then, HPW with high intrinsic ODS activity was introduced in 1 V/SiBeta to enhance the support utilization rate and create more active sites. As displayed in Fig. 3b, the ODS reaction cannot occur without catalysts, and only 3% DBT was removed without oxidants, which may be related to the adsorption of DBT by the porous SiBeta zeolite. This also indicates that the DBT removal is mainly triggered by catalytic oxidation [30]. Remarkably, 100% removal of DBT can be achieved by 2HPW-1 V/SiBeta in 60 min, which is evidently superior to that of 3 V/SiBeta and 3HPW/SiBeta. This may be related to that the dual active components in 2HPW-1 V/SiBeta are conducive to the exposure of active sites, but the excessive single active component in 3 V/SiBeta and 3HPW/SiBeta would trend to agglomerate.

To better examine the influence of reaction temperature on the ODS efficiency, the oxidation kinetics at different reaction temperatures were calculated. As shown in Fig. 3c, the reaction time and $\ln(C_t/C_0)$ exhibit a certain linear relationship with the presence of sufficient TBHP oxidants, suggesting the ODS reaction follows the pseudo-first-order kinetics. According to the formula $\ln(C_t/C_0) = k_{ODS} \cdot t$, k_{ODS} is the reaction rate constant and can be obtained from the slopes of the lines in Fig. 3c. The oxidant is very sufficient in the initial ODS reaction stage, increasing the reaction temperature can obviously enhance the reaction rate, especially in the first 10 min, indicating the more favorable reaction kinetics of high reaction temperature (Fig. 3c). However, as the ODS reaction continues, the oxidants will decompose at high temperature, leading to the decrement of reaction rate. The desulfurization activity of 2HPW-1 V/SiBeta at 70 and 80 °C are similar to that at 60 °C, all of them require 60 min to achieve 100% removal of DBT (Fig. S7). Therefore, 60 °C is the optimal reaction temperature by comprehensively considering DBT conversion and experimental cost. Besides, the catalyst dosage is another important factor that can determine the efficiency of DBT removal. As shown in Fig. 3d, the desulfurization rate is clearly enhanced with the catalyst dosage increase from 10 to 30 mg, and reaches a plateau with the catalyst dosage higher than 20 mg. Based on the comprehensive consideration of economic efficiency and catalytic performance, 60 °C and 20 mg can be the optimal reaction temperature and catalyst dosage, respectively. Noticeably, both the reaction temperature and catalytic ability of 2HPW-1 V/SiBeta have great advantages compared with recently reported HPW-based [31–35], transition metal based [5,10,17,36–38], and some dual active sites supported catalysts [39–41], as shown in Fig. 3e.

Inspired by the commendable catalytic performance of 2HPW-1 V/SiBeta for DBT oxidation, the desulfurization activity of typical refractory sulfur compounds such as BT and 4,6-DMDBT was further assessed. Fig. 3f manifests that 2HPW-1 V/SiBeta possesses excellent catalytic ODS activity for different sulfides. And the removal efficiency of different sulfides follows the order of DBT > 4,6-DMDBT > BT, which is pertinent to the low electron densities of the S atoms in BT and steric hindrance caused by methyl groups in 4,6-DMDBT, respectively [42]. Furthermore, model oils with different sulfur concentrations were used to simulate various fuel oils in practice. As expected, the 2HPW-1 V/SiBeta catalyst can achieve complete desulfurization for 500, 1000 and 2000 ppm DBT in 40, 60 and 100 min (Fig. S8), respectively, demonstrating the ascendant removal effect for various concentrations of DBT.

Series of *y*HPW-1 V/SiBeta with different loading amounts of HPW were synthesized to evaluate the optimal content of active sites in the obtained catalysts. The desulfurization activity can be dramatically enhanced by the introduction of 1% HPW, even 2HPW-1 V/SiBeta with 2% HPW can remove 100% DBT in 60 min. However, increasing the content of HPW from 3% to 12%, the catalytic performance would decrease gradually; and further enhancing the loading amount of HPW to 24%, the DBT removal efficiency of 24HPW-1 V/SiBeta can be improved again. To clearly explain the effect of HPW content on the ODS activity, schematic illustration is provided in Fig. 3g (inset). The trace amount (1%–2%) of HPW would be uniformly dispersed on the surface of the support and have no effect on the V active sites, and the synergistic catalysis between HPW and V contributes to the excellent ODS performance. Nevertheless, bulk HPW will gradually cover the V sites in the framework of SiBeta with the increasing content of HPW (Fig. S9), resulting in the decrease of desulfurization efficiency. Finally, HPW can accomplish the full coverage of all V sites and become the only active site, so further enhance the content of HPW can lead to the slight improvement of ODS activity [43].

In order to verify the feasibility of the increased support utilization rate strategy, various transition metal and HPAs were used to synthesize series of 2HPAs-1 M/SiBeta for ODS reaction. In Fig. 3h, it is obvious that the desulfurization activity of all catalysts with dual active sites (2HPAs-1 M/SiBeta) are superior to that of single active site catalysts (3HPAs/SiBeta and 3 M/SiBeta), verifying the increased support utilization rate strategy is universal. This is supported by that the two different active components can effectively avoid the agglomeration of the excessive single active sites and promote the formation of synergistic catalytic effect. When the same HPAs is introduced, the ODS activities of 2HPAs-1 M/SiBeta and M/SiBeta vary in the sequence of: 2HPAs-1 V/SiBeta > 2HPAs-1Ti/SiBeta > 2HPAs-1 Nb/SiBeta > 2HPAs-1Zr/SiBeta, which is the same as the order of the oxidizing ability, Lewis acid strength and density of these catalysts (Figs. S10 and S11) [44]. Transition metal atoms substituted into the SiBeta can induce the generation of Lewis acid sites, and the strong Lewis acidity of transition metal with high electron affinity encourages the adsorption of the lone pairs on DBT, thereby accelerating the ODS process [18].

The catalytic oxidation ability of HPAs/SiBeta in DBT removal decreases in the order of 3HPMo/SiBeta > 3HPW/SiBeta > 3HSiW/SiBeta, which is consistent with the previous report [45]. However, the ODS activity of 2HPMo-1 M/SiBeta is slightly lower than that of 2HPW-1 M/SiBeta, and there is no clear correlation between the oxidizing ability and ODS activity of 2HPAs-1 M/SiBeta (Fig. S12). This reveals that the commendable ODS catalytic performance of 2HPAs-1 M/SiBeta origins from not only the simple superposition of activity of these two active sites, but also the presence of synergistic catalytic effect. As previously reported, the coexistence of Lewis and Brønsted acid sites energetically facilitated the formation of peroxometallate complexes [39,46]. For 2HPAs-1 M/SiBeta, HPAs act as the typical Brønsted acid sites, and the acid strength and acid site density follows the trend: 2HPW-1 M/SiBeta > 2HSiW-1 M/SiBeta > 2HPMo-1 M/SiBeta and

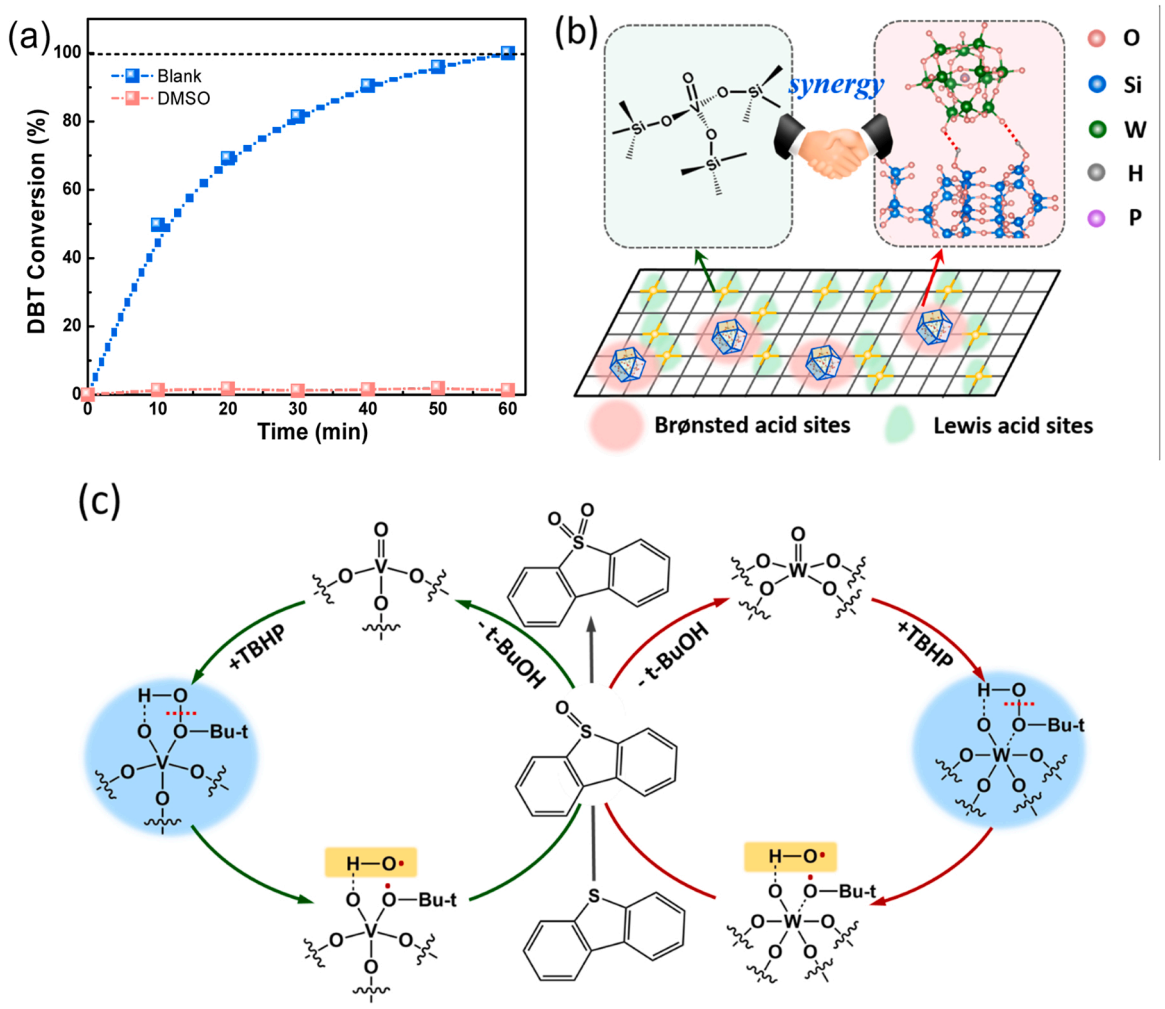

Fig. 4. (a) The inhibition effect of DMSO on the catalytic reaction over the 2HPW-1 V/SiBeta for the oxidation of DBT. (b) Illustration of the structure of 2HPW-1 V/SiBeta. (c) Proposed reaction mechanism for the catalytic oxidation of DBT on 2HPW-1 V/SiBeta.

2HPW-1 M/SiBeta > 2HPMo-1 M/SiBeta > 2HSiW-1 M/SiBeta, respectively (Figs. S13 and S14). As shown in Fig. S15, the DBT conversion correlates with the Brønsted acid sites density but not with the acid strength of 2HPAs-1 M/SiBeta with identical transition metal, indicating the maximum number of Brønsted acid site density can enhance the catalytic performance greatly. Based on the above analysis, the highest desulfurization activity of 2HPW-1 V/SiBeta among these 2HPAs-1 M/SiBeta catalysts can be ascribed to the existence of transition metal with high Lewis acid strength and density and the maximum number of Brønsted acid site density.

3.3. Exploration of reaction mechanism

To elucidate the specific reaction mechanism and active intermediates, the quenching experiment with dimethyl sulfoxide (DMSO) was performed. Compared with the blank experiment, the addition of DMSO severely suppressed the oxidation of DBT, suggesting the formation of •OH radicals during the ODS reaction (Fig. 4a). The high performance in the 2HPW-1 V/SiBeta catalyst for ODS reaction is inseparable from its unique structure. The existence of tetrahedral V species is confirmed by UV–vis spectra (Fig. 2a), and the corresponding result reveals that most of V is incorporated into the Beta zeolite framework by coordinating with silanols. The location of HPW in 2HPW-1 V/SiBeta is also detected by XPS analysis (Fig. 2c), which indicates that the bulk HPW are distributed on the surface of SiBeta by the weak interaction effect and didn't influence the exposure of V. TEM and EDS mapping images suggest that both V and HPW are highly dispersed, which induce the generation of Lewis and Brønsted acid sites, respectively, confirmed by NH_3-TPD. In light of the above characterization, the model structure of 2HPW-1 V/SiBeta can be speculated in Fig. 4b.

Furthermore, the plausible reaction mechanism for the catalytic oxidation of DBT on 2HPW-1 V/SiBeta is rationally proposed (Fig. 4c) on the basis of the above-mentioned physicochemical characterization and activity discussion. Firstly, the porous structure of 2HPW-1 V/SiBeta ensures the efficient adsorption of DBT and TBHP to make sufficient contact between the reactants and active sites. After that, the tetrahedral V and Keggin HPW active components can be irreversibly activated by TBHP to form the peroxometallate complexes (the blue regions in Fig. 4c), while the synergy between Lewis and Brønsted acid sites can further promote the above process. Specifically, Brønsted acid site can promote the electrophilic activation of oxidant toward nucleophilic substrates, and numerous Lewis acid sites can accept electron from the S atom of DBT with two pairs of isolated electrons (act as Lewis base or electron donator) by acid-base reaction pathway [39,46]. On the basis of the previous reports and the coordination environment of active metal V and W [18,24,45], it is speculated that the peroxometallate complexes may present the five-member ring structure, where V and W atoms with high electron density would transfer electrons to their adjacent O atoms, leading to the cleavage of O-O bond to generate the ·OH radicals. Finally, ·OH with strong oxidizing capability can oxidize DBT to DBTO, which can be further oxidized to $DBTO_2$ with high polarity [47]. And the products $DBTO_2$ have been detected by GC-MS

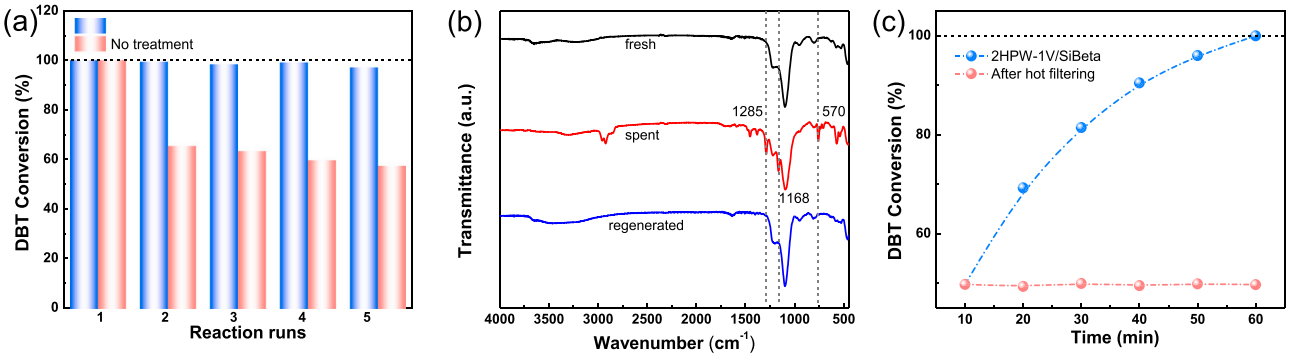

Fig. 5. (a) Recycling experiments of 2HPW-1 V/SiBeta with no treatment and wash treatment between runs. (b) FT-IR spectra of fresh, spent and regenerated 2HPW-1 V/SiBeta. (c) Leaching experiment of 2HPW-1 V/SiBeta catalyst was performed after 10 min.

shown in Fig. S16.

3.4. Evaluation of recycling performance

As the critical indicators of practical application, the recycling performance of 2HPW-1 V/SiBeta in the ODS reaction was investigated. After the ODS reaction, the catalysts were separated from oil phase by the facile centrifugation, and then dried in the 200 °C oven for 12 h. Unexpectedly, the oxidation rate of DBT with an ≈ 40% drop can be observed after the first ODS cycle (Fig. 5a). As compared with the FT-IR spectrum of the fresh 2HPW-1 V/SiBeta (Fig. 5b), the newborn peaks of the spent catalyst after the first cycle at 1285, 1168 and 570 cm^{-1} are ascribed to the characteristic vibration of -SO_2- in the $DBTO_2$ [48]. The adsorption capacity of 2HPW-1 V/SiBeta to $DBTO_2$ is highest among these components, resulting from that the silanol groups in SiBeta can coordinate with $DBTO_2$ by hydrogen bond [48]. Furthermore, the influence of catalyst dosage on the adsorption of $DBTO_2$ also has been explored; as shown in Fig. S17, the adsorption ratio of $DBTO_2$ can be achieved to 80% by 50 mg catalysts. The above analysis confirms that 2HPW-1 V/SiBeta can not only achieve the catalytic oxidation of DBT efficiently but also remove most of the corresponding products $DBTO_2$ by adsorption.

However, the main reason for the deactivation of 2HPW-1 V/SiBeta is also the adsorption effect of $DBTO_2$, which leads to the blockage of pores (Fig. S18) and the coverage of active sites. After repeated washing with ethanol, the highly polar $DBTO_2$, and a small amount of decalin and DBT were completely removed for the regenerated catalysts, as confirmed by FT-IR (Fig. 5b) and N_2 adsorption-desorption analysis (Fig. S18). In addition, the catalytic activity of regenerated 2HPW-1 V/SiBeta is capable to the initial level after five times regeneration. To exclude the re-adsorption effect of the support on the active species that have fallen off in the oil during the cold filtration, hot filtering experiment was carried out after 10 min reaction, wherein the desulfurization test continues on the filtered liquid after catalyst removal [49]. As shown in Fig. 5c, 1000 ppm of DBT can be removed completely in 60 min with the presence of 2HPW-1 V/SiBeta. Nevertheless, the DBT conversion rate hardly changed after the hot filtration, confirming that the active species didn't leach into the oil phase during the ODS reaction. Therefore, the systematic analysis and experiments provide compelling evidence that 2HPW-1 V/SiBeta have high intrinsic activity, excellent recycling performance and stability toward the ODS reaction.

4. Conclusion

The increasing support utilization rate strategy has been developed to load additional HPW on V/SiBeta with the optimal content to enhance the performance of traditional metal-based supported catalysts toward ODS reaction. V sites are bound to the silanol groups into the framework of SiBeta and HPW is anchored to silica matrix on the surface of SiBeta, especially, both of them are uniformly dispersed. The outstanding desulfurization efficiency is resulted from the high intrinsic activity of HPW and tetrahedral V species, and the synergy between Lewis and Brønsted acid sites. Furthermore, the obtained catalyst has a strong adsorption effect on the oxidation products due to the existence of abundant silanol groups, leading to the production of ultra clean fuels without further extraction step. By adjusting the types of HPAs and transition metal to control the acid strength and density, it has been found that the ODS performance can be enhanced by increasing the strength and density of Lewis acid sites and the density of and Brønsted acid sites. This work contributes a novel approach to the facile access of high performance for supported metal-based catalysts and might shed some light on the development of supported catalysts in green catalysis.

CRediT authorship contribution statement

Lei Chen: Conceptualization, Methodology, Investigation, Writing – original draft. **Jin-Tao Ren:** Formal analysis, Physicochemical characterization. **Zhong-Yong Yuan:** Supervision, Project administration, Funding acquisition.

Declaration of Competing Interest

The authors declare that they have no known competing financial interests or personal relationships that could have appeared to influence the work reported in this paper.

Acknowledgments

This work was supported by the National Natural Science Foundation of China (21875118 and 22111530112) and Tianjin Research Innovation Project for Postgraduate Students (2020YJSB147) the Ph.D. Candidate Research Innovation Fund of the NKU School of Materials Science and Engineering.

Appendix A. Supporting information

Supplementary data associated with this article can be found in the online version at doi:10.1016/j.apcatb.2021.121044.

References

[1] X.B. Lim, W.J. Ong, A current overview of the oxidative desulfurization of fuels utilizing heat and solar light: from materials design to catalysis for clean energy, Nanoscale Horiz. 6 (2021) 588–633, https://doi.org/10.1039/d1nh00127b.
[2] C. Wang, H. Li, X. Zhang, Y. Qiu, Q. Zhu, S. Xun, W. Yang, H. Li, Z. Chen, W. Zhu, Atomic-layered α-V_2O_5 nanosheets obtained via fast gas-driven exfoliation for superior aerobic oxidative desulfurization, Energy Fuels 34 (2020) 2612–2616, https://doi.org/10.1021/acs.energyfuels.9b04401.

[3] M. Hossain, H. Park, H. Choi, A comprehensive review on catalytic oxidative desulfurization of liquid fuel oil, Catalysts 9 (2019) 229, https://doi.org/10.3390/catal9030229.

[4] N.A. Khan, B.N. Bhadra, S.W. Park, Y.S. Han, S.H. Jhung, Tungsten nitride, well-dispersed on porous carbon: remarkable catalyst, produced without addition of ammonia, for the oxidative desulfurization of liquid fuel, Small (2019), 1901564, https://doi.org/10.1002/smll.201901564.

[5] K. Chen, X.-M. Zhang, X.-F. Yang, M.-G. Jiao, Z. Zhou, M.-H. Zhang, D.-H. Wang, X.-H. Bu, Electronic structure of heterojunction MoO_2/g-C_3N_4 catalyst for oxidative desulfurization, Appl. Catal. B 238 (2018) 263–273, https://doi.org/10.1016/j.apcatb.2018.07.037.

[6] G. Ye, H. Wang, W. Chen, H. Chu, J. Wei, D. Wang, J. Wang, Y. Li, In situ implanting of single tungsten sites into defective UiO-66(Zr) by solvent-free route for efficient oxidative desulfurization at room temperature, Angew. Chem. Int. Ed. 60 (2021) 20318–20324, https://doi.org/10.1002/anie.202107018.

[7] R. Abazari, L. Esrafili, A. Morsali, Y. Wu, J. Gao, PMo_{12}@UiO-67 nanocomposite as a novel non-leaching catalyst with enhanced performance durability for sulfur removal from liquid fuels with exceptionally diluted oxidant, Appl. Catal. B 283 (2021), 119582, https://doi.org/10.1016/j.apcatb.2020.119582.

[8] R. Bai, Q. Sun, Y. Song, N. Wang, T. Zhang, F. Wang, Y. Zou, Z. Feng, S. Miao, J. Yu, Intermediate-crystallization promoted catalytic activity of titanosilicate zeolites, J. Mater. Chem. A 6 (2018) 8757–8762, https://doi.org/10.1039/c8ta01960f.

[9] G. Ye, H. Wang, X. Zeng, L. Wang, J. Wang, Defect-rich bimetallic UiO-66(Hf-Zr): solvent-free rapid synthesis and robust ambient-temperature oxidative desulfurization performance, Appl. Catal. B 299 (2021), 120659, https://doi.org/10.1016/j.apcatb.2021.120659.

[10] M.A. Astle, G.A. Rance, H.J. Loughlin, T.D. Peters, A.N. Khlobystov, Molybdenum dioxide in carbon nanoreactors as a catalytic nanosponge for the efficient desulfurization of liquid fuels, Adv. Funct. Mater. 29 (2019), 1808092, https://doi.org/10.1002/adfm.201808092.

[11] L. Chen, Z.-P. Hu, J.-T. Ren, Z. Wang, Z.-Y. Yuan, Efficient oxidative desulfurization over highly dispersed molybdenum oxides supported on mesoporous titanium phosphonates, Micro Mesoporous Mat. 315 (2021), 110921, https://doi.org/10.1016/j.micromeso.2021.110921.

[12] M. Crucianelli, B.M. Bizzarri, R. Saladino, SBA-15 anchored metal containing catalysts in the oxidative desulfurization process, Catalysts 9 (2019) 984, https://doi.org/10.3390/catal9120984.

[13] J. González, J.A. Wang, L.F. Chen, M.E. Manríquez, J.M. Dominguez, Structural defects, lewis acidity, and catalysis properties of mesostructured WO3/SBA-15 nanocatalysts, J. Phys. Chem. C 121 (2017) 23988–23999, https://doi.org/10.1021/acs.jpcc.7b06373.

[14] Y. Wang, Z. Hu, W. Tian, L. Gao, Z. Wang, Z. Yuan, Framework-confined Sn in Si-beta stabilizing ultra-small Pt nanoclusters as direct propane dehydrogenation catalysts with high selectivity and stability, Catal. Sci. Technol. 9 (2019) 6993–7002, https://doi.org/10.1039/c9cy01907c.

[15] C. Chen, S. Zhang, Z. Wang, Z. Yuan, Ultrasmall Co confined in the silanols of dealuminated beta zeolite: a highly active and selective catalyst for direct dehydrogenation of propane to propylene, J. Catal. 383 (2020) 77–87, https://doi.org/10.1016/j.jcat.2019.12.037.

[16] C. Chen, Z. Hu, J. Ren, S. Zhang, Z. Wang, Z. Yuan, ZnO nanoclusters supported on dealuminated zeolite β as a novel catalyst for direct dehydrogenation of propane to propylene, ChemCatChem 11 (2019) 868–877, https://doi.org/10.1002/cctc.201801708.

[17] K. Leng, X. Li, G. Ye, Y. Du, Y. Sun, W. Xu, Ti-containing hierarchical Beta with highly active sites for deep desulfurization of fuels under mild conditions, Catal. Sci. Technol. 6 (2016) 7615–7622, https://doi.org/10.1039/c6cy01389a.

[18] D.T. Bregante, A.Y. Patel, A.M. Johnson, D.W. Flaherty, Catalytic thiophene oxidation by groups 4 and 5 framework-substituted zeolites with hydrogen peroxide: mechanistic and spectroscopic evidence for the effects of metal Lewis acidity and solvent Lewis basicity, J. Catal. 364 (2018) 415–425, https://doi.org/10.1016/j.jcat.2018.06.009.

[19] H.P. Winoto, Z.A. Fikri, J.-M. Ha, Y.-K. Park, H. Lee, D.J. Suh, J. Jae, Heteropolyacid supported on Zr-Beta zeolite as an active catalyst for one-pot transformation of furfural to γ-valerolactone, Appl. Catal. B 241 (2019) 588–597, https://doi.org/10.1016/j.apcatb.2018.09.031.

[20] Z. Xu, Y. Yue, X. Bao, Z. Xie, H. Zhu, Propane dehydrogenation over Pt clusters localized at the Sn single-site in zeolite framework, ACS Catal. 10 (2019) 818–828, https://doi.org/10.1021/acscatal.9b03527.

[21] C. Chen, M. Sun, Z. Hu, Y. Liu, S. Zhang, Z. Yuan, Nature of active phase of VO_x catalysts supported on SiBeta for direct dehydrogenation of propane to propylene, Chin. J. Catal. 41 (2020) 276–285, https://doi.org/10.1016/s1872-2067(19)63444-3.

[22] A. Held, J. Kowalska-Kuś, Y. Millot, F. Averseng, C. Calers, L. Valentin, S. Dzwigaj, Influence of the preparation procedure of vanadium-containing SiBEA zeolites on their catalytic activity in propene epoxidation, J. Phys. Chem. C 122 (2018) 18570–18582, https://doi.org/10.1021/acs.jpcc.8b05731.

[23] M. Trejda, M. Ziolek, Y. Millot, K. Chalupka, M. Che, S. Dzwigaj, Methanol oxidation on VSiBEA zeolites: influence of V content on the catalytic properties, J. Catal. 281 (2011) 169–176, https://doi.org/10.1016/j.jcat.2011.04.013.

[24] K. Chalupka, C. Thomas, Y. Millot, F. Averseng, S. Dzwigaj, Mononuclear pseudo-tetrahedral V species of VSiBEA zeolite as the active sites of the selective oxidative dehydrogenation of propane, J. Catal. 305 (2013) 46–55, https://doi.org/10.1016/j.jcat.2013.04.020.

[25] Y. Du, L. Zhou, Z. Guo, X. Du, J. Lei, Preparation of ordered meso/macroporous HPW/titania–silica catalyst for efficient oxidative desulfurization of model fuel, J. Porous Mater. 26 (2018) 1069–1077, https://doi.org/10.1007/s10934-018-0701-5.

[26] X. You, L.-l Yu, F.-f Xiao, S.-c Wu, C. Yang, J.-h Cheng, Synthesis of phosphotungstic acid-supported bimodal mesoporous silica-based catalyst for defluorination of aqueous perfluorooctanoic acid under vacuum UV irradiation, Chem. Eng. J. 335 (2018) 812–821, https://doi.org/10.1016/j.cej.2017.10.123.

[27] H. Wang, I. Jibrin, X. Zeng, Catalytic oxidative desulfurization of gasoline using phosphotungstic acid supported on MWW zeolite, Front. Chem. Sci. Eng. 14 (2019) 546–560, https://doi.org/10.1007/s11705-019-1842-z.

[28] Y. Du, L. Zhou, Z. Liu, J. Lei, Hierarchical porous HPW/titania–silica material with superior adsorption-catalytic oxidation activity for multi-ring thiophenic sulfur compounds, N. J. Chem. 44 (2020) 4942–4951, https://doi.org/10.1039/c9nj05793e.

[29] W. Zhang, W. Hou, T. Meng, W. Zhuang, J. Xie, Y. Zhou, J. Wang, Direct synthesis of V-containing all-silica beta-zeolite for efficient one-pot, one-step conversion of carbohydrates into 2,5-diformylfuran, Catal. Sci. Technol. 7 (2017) 6050–6058, https://doi.org/10.1039/c7cy01834g.

[30] L. Chen, J.-T. Ren, Z.-Y. Yuan, Atomic heterojunction-induced electron interaction in P-doped g-C_3N_4 nanosheets supported V-based nanocomposites for enhanced oxidative desulfurization, Chem. Eng. J. 387 (2020), 124164, https://doi.org/10.1016/j.cej.2020.124164.

[31] X. Zhang, Y. Zhu, P. Huang, M. Zhu, Phosphotungstic acid on zirconia-modified silica as catalyst for oxidative desulfurization, RSC Adv. 6 (2016) 69357–69364, https://doi.org/10.1039/c6ra16622a.

[32] H. Yang, B. Jiang, Y. Sun, L. Zhang, Z. Huang, Z. Sun, N. Yang, Heterogeneous oxidative desulfurization of diesel fuel catalyzed by mesoporous polyoxometallate-based polymeric hybrid, J. Hazard. Mater. 333 (2017) 63–72, https://doi.org/10.1016/j.jhazmat.2017.03.017.

[33] S. Ribeiro, A.D.S. Barbosa, A.C. Gomes, M. Pillinger, I.S. Gonçalves, L. Cunha-Silva, S.S. Balula, Catalytic oxidative desulfurization systems based on Keggin phosphotungstate and metal-organic framework MIL-101, Fuel Process. Technol. 116 (2013) 350–357, https://doi.org/10.1016/j.fuproc.2013.07.011.

[34] B. Li, Z. Liu, J. Liu, Z. Zhou, X. Gao, X. Pang, H. Sheng, Preparation, characterization and application in deep catalytic ODS of the mesoporous silica pillared clay incorporated with phosphotungstic acid, J. Colloid Interface Sci. 362 (2011) 450–456, https://doi.org/10.1016/j.jcis.2011.07.025.

[35] H. Ji, J. Sun, P. Wu, B. Dai, Y. Chao, M. Zhang, W. Jiang, W. Zhu, H. Li, Deep oxidative desulfurization with a microporous hexagonal boron nitride confining phosphotungstic acid catalyst, J. Mol. Catal. A: Chem. 423 (2016) 207–215, https://doi.org/10.1016/j.molcata.2016.06.019.

[36] W. Jin, Y. Tian, G. Wang, D. Zeng, J. Cui, Q. Xu, Ultra-deep oxidative desulfurization of fuel with H_2O_2 catalyzed by molybdenum oxide supported on alumina modified by Ca^{2+}, RSC Adv. 7 (2017) 48208–48213, https://doi.org/10.1039/c7ra08900g.

[37] N. Afzali, R. Kardanpour, F. Zadehahmadi, S. Tangestaninejad, M. Moghadam, V. Mirkhani, A. Mechler, I. Mohammadpoor-Baltork, M. Bahadori, Molybdenum (VI)-functionalized UiO-66 provides an efficient heterogeneous nanocatalyst in oxidation reactions, Appl. Organo Chem. 33 (2019), https://doi.org/10.1002/aoc.5225.

[38] R. Ma, J. Guo, D. Wang, M. He, S. Xun, J. Gu, W. Zhu, H. Li, Preparation of highly dispersed WO_3/few layer g-C_3N_4 and its enhancement of catalytic oxidative desulfurization activity, Colloids Surf. A Physicochem. Eng. Asp. 572 (2019) 250–258, https://doi.org/10.1016/j.colsurfa.2019.04.006.

[39] Q. Luo, Q. Zhou, Y. Lin, S. Wu, H. Liu, C. Du, Y. Zhong, C. Yang, Fast and deep oxidative desulfurization of dibenzothiophene with catalysts of MoO_3–TiO_2@MCM-22 featuring adjustable Lewis and Brønsted acid sites, Catal. Sci. Technol. 9 (2019) 6166–6179, https://doi.org/10.1039/c9cy01438a.

[40] M.A. Alvarez-Amparán, L. Cedeño-Caero, MoO_x-VO_x based catalysts for the oxidative desulfurization of refractory compounds: influence of MoO_x-VO_x interaction on the catalytic performance, Catal. Today 282 (2017) 133–139, https://doi.org/10.1016/j.cattod.2016.07.002.

[41] M.L. Luna, M.A. Alvarez-Amparán, L. Cedeño-Caero, Performance of WO_x–VO_x based catalysts for ODS of dibenzothiophene compounds, J. Taiwan Inst. Chem. Eng. 95 (2019) 175–184, https://doi.org/10.1016/j.jtice.2018.06.010.

[42] A. Rajendran, T. Cui, H. Fan, Z. Yang, J. Feng, W. Li, A comprehensive review on oxidative desulfurization catalysts targeting clean energy and environment, J. Mater. Chem. A 8 (2020) 2246–2285, https://doi.org/10.1039/c9ta12555h.

[43] A.K. Dizaji, B. Mokhtarani, H.R. Mortaheb, Deep and fast oxidative desulfurization of fuels using graphene oxide-based phosphotungstic acid catalysts, Fuel 236 (2019) 717–729, https://doi.org/10.1016/j.fuel.2018.09.076.

[44] D.T. Bregante, D.W. Flaherty, Periodic trends in olefin epoxidation over group IV and V framework-substituted zeolite catalysts: a kinetic and spectroscopic study, J. Am. Chem. Soc. 139 (2017) 6888–6898, https://doi.org/10.1021/jacs.7b01422.

[45] R. Ghubayra, C. Nuttall, S. Hodgkiss, M. Craven, E.F. Kozhevnikova, I. V. Kozhevnikov, Oxidative desulfurization of model diesel fuel catalyzed by carbon-supported heteropoly acids, Appl. Catal. B 253 (2019) 309–316, https://doi.org/10.1016/j.apcatb.2019.04.063.

[46] G. Rodriguez-Gattorno, A. Galano, E. Torres-García, Surface acid–basic properties of WO_x–ZrO_2 and catalytic efficiency in oxidative desulfurization, Appl. Catal. B 92 (2009) 1–8, https://doi.org/10.1016/j.apcatb.2009.07.031.

[47] X. Chang, X.F. Yang, Y. Qiao, S. Wang, M.H. Zhang, J. Xu, D.H. Wang, X.H. Bu, Confined heteropoly blues in defected Zr-MOF (bottle around ship) for high-

efficiency oxidative desulfurization, Small 16 (2020), 1906432, https://doi.org/10.1002/smll.201906432.
[48] H. Wang, C. Shi, S. Chen, R. Chen, P. Sun, T. Chen, Hierarchically mesoporous titanosilicate single-crystalline nanospheres for room temperature oxidative–adsorptive desulfurization, ACS Appl. Nano Mater. 2 (2019) 6602–6610, https://doi.org/10.1021/acsanm.9b01496.
[49] L. Kang, H. Liu, H. He, C. Yang, Oxidative desulfurization of dibenzothiophene using molybdenum catalyst supported on Ti-pillared montmorillonite and separation of sulfones by filtration, Fuel 234 (2018) 1229–1237, https://doi.org/10.1016/j.fuel.2018.07.148.